RSC Advances

ROYAL SOCIETY OF CHEMISTRY

www.rsc.org/advances

Journal Name

RSCPublishing

ARTICLE

Fabrication of Polypyrrole Nanoplates Decorated with Silver and Gold Nanoparticles for Sensor Applications

Junwei Ding[a], Kai Zhang[a], Gang Wei,[b*] Zhiqiang Su[a*]

Cite this: DOI: 10.1039/xoxxoooooox

Received ooth January 2012,
Accepted ooth January 2012

DOI: 10.1039/xoxxoooooox

www.rsc.org/

Polypyrrole nanoplates (PPyNPTs) were successfully synthesized via in-situ chemical oxidation polymerization of pyrrole molecules. Furthermore, silver and gold nanoparticles (Ag and AuNPs) were assembled onto the as-prepared PPyNPTs by electrostatic interaction to fabricate two nanohybrids of PPyNPT-Ag and PPyNPT-Au, and their structures were characterized by scanning electron microscopy, transmission electron microscopy, Fourier transform infrared spectroscopy, and X-ray diffraction. The optimal parameters for creating uniform PPyNPT-Ag and PPyNPT-Au nanohybrids were obtained by controlling the reactive conditions, and the created PPyNPT-Ag and PPyNPT-Au nanohybrids were then immobilized onto glassy carbon electrodes and applied to construct hydrogen peroxide (H_2O_2) and dopamine (DA) sensors. We found that the fabricated sensors with PPyNPT-Ag and PPyNPT-Au nanohybrids are highly specific for sensing H_2O_2 and DA, respectively. The PPyNPT-Ag based H_2O_2 sensor exhibited a fast amperometric response to H_2O_2 with a linear range from 0.01 mM to 3.01 mM and a detection limit of 1.8 μM, and the PPyNPT-Au based DA sensor has a linear detection range from 1 μM to 5.201 mM and a detection limit of 0.36 μM.

1. Introduction

Conducting polymers (CPs) are suitable host matrices due to their advantages of permitting a facile electronic charge flow through the polymer matrix in electrochemical processes.[1-3] Polypyrrole (PPy), is one of the most promising CPs because of its ease of synthesis, good redox property, high conductivity, and excellent environmental stability.[4] The presence of conjugated double bonds along the backbone of the polymer chain with unusually low ionization potentials and high electron affinities are basic requirements for the special electrical properties of PPy. The electronic conductivity of PPy can be enhanced by a doping process resulting in incorporation of counterions such as inorganic cations and anions, organic molecules, etc.[5] The unique properties of CPs open new possibilities for technological applications, including rechargeable batteries, chemical or biochemical sensors, and polymer-based electronic devices (e.g., field-effect resistors, light emitting diodes, and solar cells), due to the high nonlinear optical properties and the electrical properties inherent to metals or semiconductors and the mechanical properties of conventional polymers. [6-10] At the same time, metallic nanoparticles (MNPs), such as silver nanoparticles (AgNPs) and gold nanoparticles (AuNPs), have been extensively used to fabricate different kinds of sensors.[11-16]

CPs have also been used as versatile matrices to embed or disperse MNPs to create composite materials possessing properties of the individual components with a synergistic effect. The combination of MNPs with CPs offers an attractive route to reinforce the polymer as well as to introduce electronic properties based on morphological modification or electronic interaction between the two components. The soft polymer matrix can accommodate an internal stress and can undergo severe volume change from the composite materials.[17] The properties of CP-MNP composites are even enhanced when the material size is reduced to the nanoscale.[18, 19] Furthermore, it was found that the conductivity and sensing behavior of CPs could be further improved by imbedding MNPs into polymer matrix to form the CP-MNP composites.[20, 21] Previously, many methods have been used to synthesize PPy-MNP nanocomposites.[22-25] For example, Lim et al. prepared PPy-Au micro- and nanostructures by electropolymerization and electro-deposition.[24] Hou et al. reported the synthesis of PPy-Ag nanocomposite by using the redox reaction of silver nitrate and pyrrole via interface polymerization.[22] Chen et al. reported a one-step process to fabricate Ag-PPy coaxial nanocables.[25] Pintér et al. reported the characterization of PPy-Ag nanocomposites prepared in the presence of different dopants.[23] To enhance the performance of the fabricated CP-MNP based sensors, two important factors should be considered. The first

one is that CPs should have the ordered structure (like nanotube, nanowire, and nanoplate), and the second one is that MNPs should uniformly distribute on the surface of CPs.[26]

It is well known that dopamine (DA) is one of the most important catecholamine neurotransmitters in the mammalian central nervous system. Previously many attempts, such as fluorometric and chromatographic techniques, have been made to detect DA.[27, 28] Electrochemical techniques showed good performance due to the advantages such as high selectivity, high sensitivity, and relative low detection limit.[29-32] Meanwhile, the detection of H_2O_2 is also very important because H_2O_2 is a main product of enzymatic reactions.[33] The electrochemical detection of H_2O_2 was introduced to achieve a lower detection limit and lower cost compared to other detection methods.[34-38] Herein, we reported the synthesis of PPy nanoplates (PPyNPTs) by the in-situ polymerization of pyrrole (Py). Furthermore, the as-prepared AgNPs and AuNPs were successfully self-assembled onto the PPyNPTs to synthesize functional PPyNPT-Ag and PPyNPT-Au nanohybrids, respectively. Both nanohybrids were utilized to modify glass carbon electrode (GCE) for the fabrication of H_2O_2 and DA sensors. We found that the PPyNPT-Ag and PPyNPT-Au modified GCEs showed enhanced electrocatalytic activity for the reduction of H_2O_2 and oxidation of DA compared to PPyNPTs modified GCE, and the sensors based on PPyNPT-Ag and PPyNPT-Au have unique sensing ability on H_2O_2 and DA, respectively.

2. Experimental

2.1 Reagents

Ascorbic acid (AA), uric acid (UA), DA, and glucose were obtained from J &K Scientific Ltd. (Beijing, China). Disodium hydrogen phosphate (Na_2HPO_4), sodium dihydrogen phosphate (NaH_2PO_4), sodium borohydride ($NaBH_4$), silver nitrate ($AgNO_3$), absolute ethyl alcohol were purchased from Beijing Chemicals Co., Ltd. (Beijing, China). Py was distilled under vacuum before use and other reagents were used as received. The water used was purified through a Millipore system (~18.2 MΩ·cm).

2.2 Preparation of PPyNPTs

0.17 g of Py was added to 85 mL deionized water. The mixture was stirred until the Py was thoroughly dissolved. After that, 0.6 g of ammonium peroxydisulfate (APS) as oxidant was added to the above solution. The obtained mixture was allowed to react for 12 h under constant stirring at room temperature, and the resultant product was centrifuged and dried.

2.3 Preparation of PPyNPT-Ag and PPyNPT-Au

AgNPs were synthesized through a developed strategy based on previous report.[39] Briefly, 2.5 mL of $AgNO_3$ solution (0.01 M) was added to 75 mL deionized water under stirring. After 10 min, 5 mL of mercaptocarboxylic acid (MA) solution (0.01 M) was added to the mixed solution and 2.5 mL of NaI solution (0.01 M) was added into the mixed solution under vigorous stirring. After 20 min of further reaction, 25 mg $NaBH_4$ was added and the mixture was kept stirred for another 30 min until a light red colloid of Ag NPs appeared.

The Au colloid was prepared according to previous report.[40] In brief, 100 mL of chloroauric acid solution (0.01 wt%) was heated to boiling, and then quickly added to 2.5 mL sodium citrate solution (1 wt%), continued to boil for 5 minutes.

0.05g PPyNPTs was added to the above 50 mL MA-capped AgNPs solution under stirring at room temperature. The reaction was allowed to proceed for 12 h, and the resultant product was centrifuged and dried. AgNPs could be bound onto the surface of PPyNPTs, leading to the formation of PPyNPT-Ag nanohybrids. The preparation of PPyNPT-Au nanohybrids was similar to that of PPyNPT-Ag.

To investigate the effect of different reaction parameters, such as temperature, volume of MNPs for the assembly, and the reaction period, on the formation of PPyNPT-Ag and PPyNPT-Au nanohybrids, the temperature was set from room temperature to 50, 70, and 90 °C; the volume of MNPs (AuNPs and AgNPs) was kept from 100 to 150 and 200 mL; the reaction period was adjusted from 24 to 36 and 72 h.

2.4 Electrochemical measurements

All electrochemical measurements were performed on a CHI760D electrochemical workstation (CH Instruments, Shanghai, China) at room temperature. A conventional three-electrode cell was used, including a glass carbon electrode (GCE, 3 mm in diameter) as the working electrode, an Ag/AgCl electrode (saturated KCl) as the reference electrode, and a Pt wire as auxiliary electrode. The test solutions were phosphate buffer solutions (PBS, 0.1 M), which was prepared with 0.2 M Na_2HPO_4 and 0.2 M NaH_2PO_4 and H_2SO_4 (pH=1), and deoxygenated with high-purity nitrogen for 30 minutes before electrochemical experiments.

The GCE was polished with 1 and 0.3 μm alumina powder and washed with distilled water, followed by sonication in ethanol solution and distilled water, respectively. Then, the cleaned GCE was dried with a high-purity nitrogen steam for next modification. A total of 5 μL of sample solution (1.0 mg/mL) was dropped on the GCE surface and dried at room temperature. Finally, 5 μL Nafion solution (0.1 %, diluted with ethanol) was cast onto the electrode to avoid the leakage of modified GCE.

2.5 Characterization techniques

SEM experiments were performed on JSM-6700F scanning electron microscope (JEOL). Transmission electron microscopy (TEM) experiments were performed on a TecnaiG220 transmission electron microscope (FEI) with an accelerating voltage of 200 kV. Fourier transform infrared spectroscopy (FTIR, Nicolet 6700, Thermo-Fisher), and X-ray diffraction (XRD, Rigaku D/max-2500 VB+/PC) were utilized for the characterizations of samples.

3. Results and discussion

3.1 Optimal preparation of PPyNPT-Au nanohybrids

To obtain the optimal parameters for creating uniform PPyNPT-Ag and PPyNPT-Au nanohybrids, different volumes of MNPs, reaction periods, and reaction temperatures were tested. For the simplicity, here we focus on the optimal preparation of PPyNPT-Au nanohybrids.

Fig. 1a-c shows the effect of different volumes of AuNPs on the formation of PPyNPT-Au nanohybrids. The SEM images in Fig. 1a and b indicate that, as the volume of Au colloid solution increases from 100 to 150 mL, the amount of AuNPs assembled onto the as-prepared PPyNPTs by electrostatic interaction also increases. However, as the volume of Au colloid solution increases from 150 to 200 mL, the amount of AuNPs assembled onto the as-prepared PPyNPTs by electrostatic interaction is almost unchanged (as shown in Fig. 1b and c). Meanwhile, the above SEM result is in consistence with the corresponding Energy dispersive X-ray spectroscopy analysis (the weight percents of Au M in Fig. 1a-c are 6.18, 6.85, and 6.78, respectively).Based on the above result, it can be found that with the increase of the volume of Au colloid solution, the amount of AuNPs assembled onto the as-prepared PPyNPTs by electrostatic interaction will first increase and then reach a stable maximum value. We suggest that this phenomenon may be due to the amount of AuNPs assembled onto the as-prepared PPyNPTs by electrostatic interaction has a maximum value for 0.05g PPyNPTs. Therefore, a suitable volume (150 mL) of AuNPs was selected for the optimal synthesis of uniform PPyNPT-Au nanohybrids.

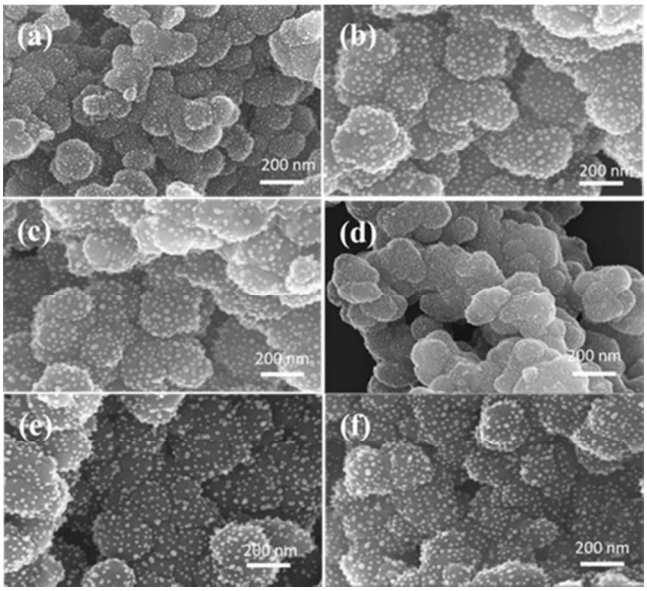

Fig. 1 Effects of different volumes of AuNPs (a-c) and reaction periods (d-f) on the formation of PPyNPT-Au nanohybrids. The volume was set to be (a) 100, (b) 150, and (c) 200 mL, respectively; the corresponding reaction condition is room temperature for 36 h. The reaction period was adjusted to be (d) 24, (e) 36, and (f) 72 h; the corresponding reaction condition is room temperature and 150 mL AuNPs.

Fig. 1d-f presents the effect of different reaction periods on the formation of PPyNPT-Au nanohybrids. The SEM images in Fig. 1d and e indicate that, as the reaction time increases from 24 to 36 h, the amount of AuNPs assembled onto the as-prepared PPyNPTs by electrostatic interaction also increases. However, as the reaction time increases from 36 to 72 h, the amount of AuNPs assembled onto the as-prepared PPyNPTs by electrostatic interaction is almost unchanged (as shown in Fig. 1e and f). The above SEM result is in consistence with the corresponding Energy dispersive X-ray spectroscopy analysis (the weight percents of Au M in Fig. 1d-f are 5.81, 6.85, and 6.76, respectively). Therefore, a better reaction period of 36 h was selected for the further synthesis of PPyNPT-Au nanohybrids.

Fig. 2 indicates the temperature effect on the formation of PPyNPT-Au nanohybrids. For this part of control experiment, 150 mL AuNPs was used and a reaction period of 36 h was fixed. The SEM images in Fig. 2a-c indicate that the amount of AuNPs assembled onto the as-prepared PPyNPTs by electrostatic interaction increases with the reaction temperature increases from room temperature to 50 and 70°C. However, as the reaction temperature increases from 70 to 90°C, the amount of AuNPs assembled onto the as-prepared PPyNPTs by electrostatic interaction decreases (as shown in Fig. 2c and d). Meanwhile, the above SEM result is also in consistence with the corresponding Energy dispersive X-ray spectroscopy analysis (the weight percents of Au M in Fig. 2a-d are 6.85, 7.13, 7.42, and 5.72, respectively).

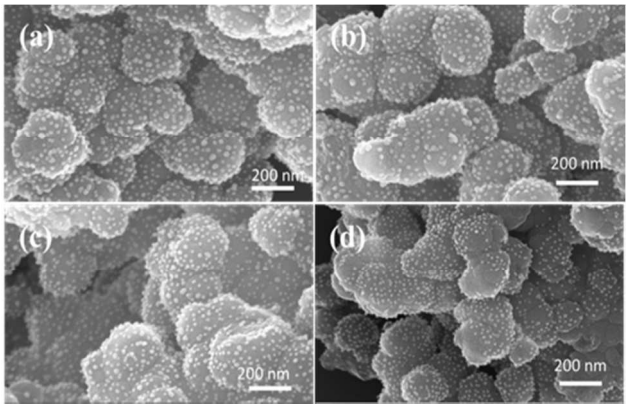

Fig. 2 Temperature effect on the formation of PPyNPT-Au nanohybrids: (a) room temperature, (b) 50, (c) 70 and (d) 90 °C. The corresponding reaction condition is 150 mL AuNPs and 36 h reaction period.

Based on the above SEM results, a relative optimal reaction parameter (150 mL MNPs, 36 h reaction period, and 70°C reaction temperature) was applied for the assembly of MNPs onto PPyNPTs and the final synthesis of PPyNPT-Ag and PPyNPT-Au nanohybrids.

3.2 Characterization of PPyNPTs, PPyNPT-Ag, and PPyNPT-Au

Fig. 3 shows the proposed mechanism for the synthesis of PPyNPTs and the subsequent fabrication of PPyNPT-Ag and

PPyNPT-Au nanohybrids. Firstly, APS was added to the system for inducing the polymerization of Py molecules and the formation of PPyNPTs. Secondly, MA-capped AgNPs and sodium citrate-capped AuNPs were assembled onto the as-prepared PPyNPTs by electrostatic interaction to fabricate nanohybrids of PPyNPT-Ag and PPyNPT-Au.[41, 42]

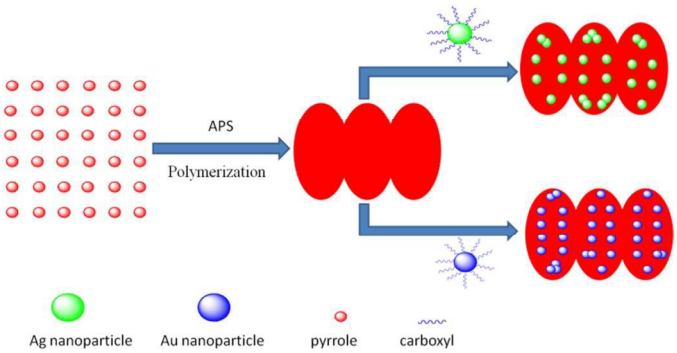

Fig. 3 Schematic representations for the synthesis of PPyNPTs, PPyNPT-Ag, and PPyNPT-Au nanohybrids.

The samples of PPyNPTs, PPyNPT-Ag, and PPyNPT-Au were characterized with XRD and FTIR firstly, and the results are shown in Fig. 4a and b. The XRD pattern of PPyNPT-Ag confirmed the successful assembly of AgNPs onto the surface of PPyNPTs. The broad peak with 2θ around 23.6° is assigned to the diffraction of amorphous PPy and other peaks with 2θ at 39.2° is related to the [111] diffraction of Ag and 2θ at 42.6° and 46.2° are related to [200] diffraction of Ag, respectively. Crystallite sizes were calculated using Scherrer's equation.[43] The calculated average size of the silver is ca. 10 nm. The powder XRD analysis was also used to confirm the existence of Au in the synthesized PPyNPT-Au nanohybrids. XRD peaks appeared at 2θ of 38.3°, 44.5°, 64.7° and 77.7°, which can be assigned to the diffraction from the [111], [200], [220], and [311] crystal planes of the face-centered cubic Au structures, respectively. The size of AuNPs in the PPyNPT-Au nanohybrids has been calculated using Scherrer's formula and the value was found to be ca. 28 nm. However, it should be noted that the width and intensity of the peaks for PPyNPTs changed in the synthesized PPyNPT-Ag and PPyNPT-Au nanohybrids and appeared three diffraction peaks in the range of 20-30° for PPyNPT-Ag and PPyNPT-Au, which may due to the binding of PPyNPTs with MNPs.

Fig. 4b shows the typical FTIR spectra of PPyNPTs, PPyNPT-Ag and PPyNPT-Au. The peaks at around 1560 and 1480 cm^{-1} are assigned to the antisymmetric ring stretching mode and symmetric mode of Py ring.[44, 45] A large and descending baseline appears in the spectral region of 1700-2800 cm^{-1}, which is attributed to the free-electron conduction in PPy.[46] Previously, Martin *et al.* have reported that longer conjugation length critically led to higher conductivity and experimentally the effective conjugation length was inversely proportional to the ratio of the peak areas at 1560 and 1470 cm^{-1} (A_{1560}/A_{1470}).[47] In our work, the A_{1560}/A_{1470} values were calculated to be approximately 3.24, 2.06, and 1.16 for PPyNPTs, PPyNPT-Ag, and PPyNPT-Au, respectively. The peak ratio indicates that the PPyNPT-Ag and PPyNPT-Au nanohybrids have longer effective conjugation lengths than the created PPyNPTs.

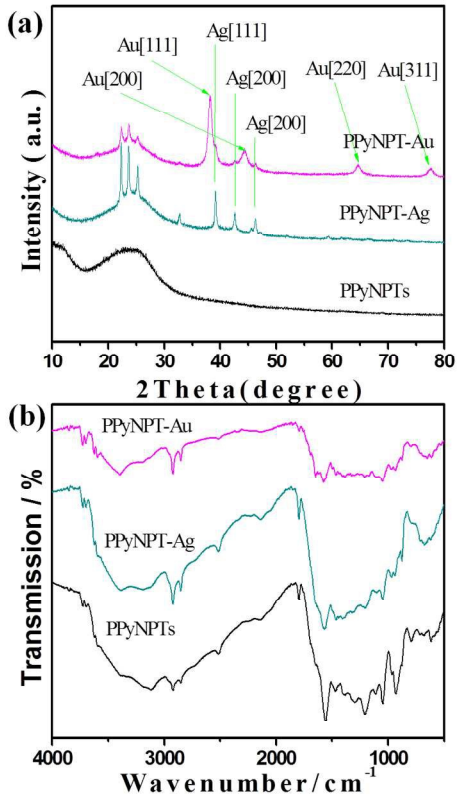

Fig. 4 (a) XRD patterns and (b) FTIR spectra of PPyNPTs, PPyNPT-Ag, and PPyNPT-Au.

The synthesized PPyNPTs, PPyNPT-Ag, and PPyNPT-Au nanohybrids were then characterized with SEM and TEM. The SEM images in Fig. 5a, c and e indicate that these products have clear plate nanostructure. Fig. 5b gives the TEM image of the PPyNPTs. It can be found that the PPyNPTs were successfully synthesized. Fig. 5d shows the TEM and HR-TEM images of the synthesized PPyNPT-Ag nanohybrids. It is clear that the AgNPs were assembled onto the surface of PPyNPTs with a mean diameter of ca. 10 nm, which is agreed with the above XRD result. Fig. 5f gives the TEM and HR-TEM images of the created PPyNPT-Au nanohybrids. It can be seen that AuNPs are on the surface of PPyNPTs with a mean diameter of ca. 30 nm, which is similar to the formation of PPyNPT-Ag nanohybrids.

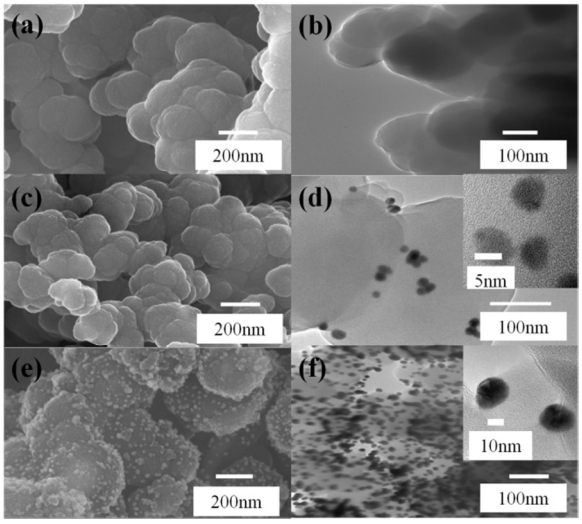

Fig. 5 Morphological characterizations: (a, c, e) typical SEM images and (b, d, f) corresponding TEM images of (a, b) PPyNPTs, (c, d) PPyNPT-Ag nanohybrids, and (e, f) PPyNPT-Au nanohybrids. The insets (d, f) are the corresponding HR-TEM images.

3.3 Electrochemical H_2O_2 sensor

To evaluate the sensing application of the synthesized PPyNPT-Ag nanohybrids, we designed a nonenzymatic H_2O_2 sensor.

Fig. 6a shows the cyclic voltammograms (CVs) of GCEs modified with Ag NPs, PPyNPTs and PPyNPT-Ag toward the reduction of H_2O_2 in the presence of 10 mM H_2O_2. The PPyNPT-Ag/GCE exhibits a notable current peak centered at -0.91 V. It can be seen that AgNPs/GCE showed better response to H_2O_2 compared to PPyNPT-Ag/GCE. However, we found that the AgNPs are very easy to fall off from the surface of GCE, and current loss is serious. In addition, the response of PPyNPTs/GCE toward the reduction of H_2O_2 is very small. So we chose the PPyNPT-Ag/GCE as the catalytic electrode for H_2O_2 reduction.

Fig. 6b shows the typical I-T plot of the PPyNPT-Ag/GCE. Although the PPyNPT-Ag/GCE exhibited the biggest response signal at −0.91 V, we determined the H_2O_2 at −0.34 V. Such a low applied potential can ensure sufficient current response with lower background or less interference of other electroactive species in the solution.[48] Fig. 6c shows the calibration curve of the sensor. The linear detection range of this H_2O_2 sensor is estimated to be from 0.01 mM to 3.01 mM (r=0.996), and the detection limit is calculated to be 1.8 μM (S/N = 3). As can be seen from Table 1, our sensor has the acceptable wide linear range and low detection limit compared with the previous H_2O_2 sensors. The selectivity test of PPyNPT-Ag modified GCE was conducted at the working potential of -0.34V. After a stable baseline, 0.1 mM H_2O_2, 0.1 mM AA, 0.1 mM UA, 0.1 mM DA, and 5 mM glucose were successively added in N_2 saturated PBS (0.1 M, pH=7.4), respectively. It can be found that negligible interference was observed at the applied potential, as shown in Fig. 6d.

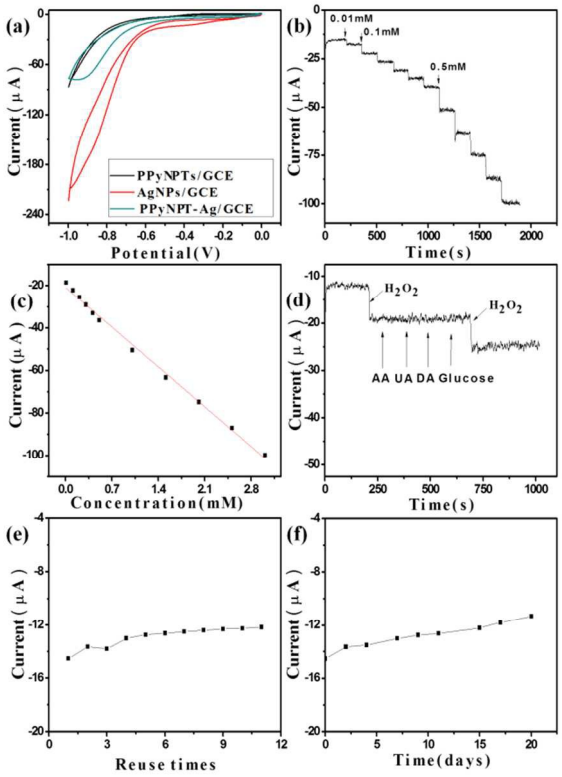

Fig. 6 H_2O_2 sensor: (a) CVs of GCEs modified with Ag NPs, PPyNPTs and PPyNPT-Ag; (b) I–T response of GCE modified with PPyNPT-Ag in 0.1 M PBS (pH 7.4); (c) The calibration curve of H_2O_2 sensor; (d) Selectivity; (e) Reuse ability, and (f) Long-term stability.

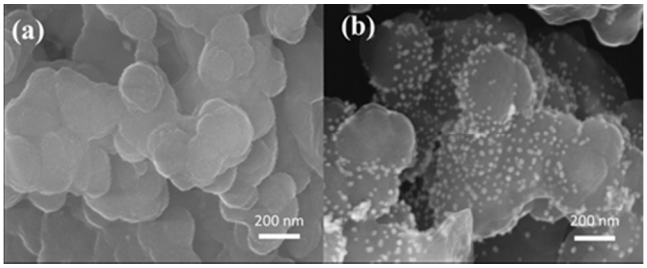

Fig. 7 SEM images of (a) PPyNPT-Ag and (b) PPyNPT-Au after 20 days electrochemical tests.

The reuse stability of the PPyNPT-Ag modified GCE was assessed by amperometry in the presence of 0.1mM of H_2O_2. The result indicates that the current of the PPyNPT-Ag modified GCE kept stable between -12 and -15 μA for at least 11 tests (Fig. 6e). The long-term stability of the PPyNPT-Ag modified GCE was also explored in the presence of 0.1mM of H_2O_2. The fabricated GCE was stored in the refrigerator at 4 °C and measured every 2-4 days over a 20-days period. The result shows that the current response maintains more than 88 % of its initial value in response to 0.1 mM H_2O_2 after 20 days, indicating an acceptable stability of our PPyNPT-Ag based sensor (shown in Fig. 6f). Meanwhile, the morphological characterization of PPyNPT-Ag after 20 days electrochemical tests is shown in Fig. 7a. As can be seen from the obtain SEM

image, the basic morphology of the PPyNPT-Ag does not change, which indicates that the prepared PPyNPT-Ag nanohybrids are very stable for long-term test.

Table.1. Comparison of the H_2O_2 sensor performances of the PPyNPT-Ag nanohybrids with previous H_2O_2 sensors.

Electrode materials	Potential (V)	Linear range (mM)	LOD (μ M)	Ref
Stable AgNPs	-0.3	0.1-180	33.9	[49]
Ag-PPy colloids	-0.3	0.1-90	1.05	[50]
Ag-thin PPy	-0.35	0.1-90	0.57	[51]
Ag-polyurethane	-0.34	0.5-30	18.6	[12]
Ag-graphene	-0.6	0.05-5	10.4	[52]
PPyNPT-Ag	-0.34	0.01-3.01	1.8	this work

3.4 Electrochemical DA sensor

In a further step, we designed a nonenzymatic DA sensor with the created PPyNPT-Au nanohybrids. The effect of the potential scanning rate (V) on the peak current for the PPyNPT-Au/GCE was measured in the range of 50-500 mV s^{-1}, as shown in Fig. 8a. The anodic peak current for PPyNPT-Au is increased linearly with the square root of the scanning rate ($V^{1/2}$), indicating that the peak current is diffusion controlled.[53] The CVs of the AuNPs, PPyNPTs, and PPyNPT-Au/GCE in the presence of 1 mM DA are shown in Fig. 8b. For the PPyNPT-Au/GCE, the redox peaks appear at 0.54 and 0.38 V, respectively, which are attributed to the oxidation/reduction of DA to dopaminequinone with participation of two electrons.[54] Previous study indicated that the electrocatalytic effect of AuNPs on the oxidation of DA is related to the size of AuNPs.[55] An optimal size of AuNPs with the maximal catalytic efficiency was found to be about 30 nm. Therefore, in this work, AuNPs with a diameter of 30 nm were used to modify the synthesized PPyNPTs and create PPyNPT-Au nanohybrids. The I-T curve is recorded at 0.63 V (as shown in Fig. 8c). The PPyNPT-Au/GCE displayed increasing amperometric responses to DA with a linear range from 1 μM to 5.201 mM (r=0.994) and a detection limit of 0.36 μM (S/N=3). As can be seen from Table 2, our sensor has the acceptable wide linear range and low detection limit compared with the previous DA sensors. The selectivity test of PPyNPT-Au modified GCE was completed at the working potential of 0.63V. After a stable baseline, 0.1 mM DA, 0.1 mM AA, 0.1 mM UA, 0.1 mM H_2O_2 were successively added in N_2 saturated H_2SO_4 (pH=1), respectively. It can also be seen that negligible interference was observed at the applied potential (as shown in Fig. 8d).

The reuse stability of the PPyNPT-Au modified GCE was assessed by amperometry in the presence of 0.1 mM DA. The result indicates that the current of the PPyNPT-Au modified GCE kept stable between -1 and -2 μA for at least 13 tests (as shown in Fig. 8e). The long-term stability of the PPyNPT-Au modified GCE was also explored in the presence of 0.1 mM DA. The fabricated GCE was stored in the refrigerator at 4 °C and measured every 2-4 days over a 20-day period. The result shows that the current response maintains more than 90 % of its initial value in response to 0.1 mM DA after 20 days, indicating an acceptable stability of our PPyNPT-Au based sensor (Fig. 8f). Meanwhile, the morphological characterization of PPyNPT-Au nanohybrids after 20 days electrochemical tests is shown in Fig. 7b. As can be seen from the obtained SEM image, the basic morphology of the PPyNPT-Au does not change, which indicates that the prepared PPyNPT-Au nanohybrids are also very stable for the long-term test.

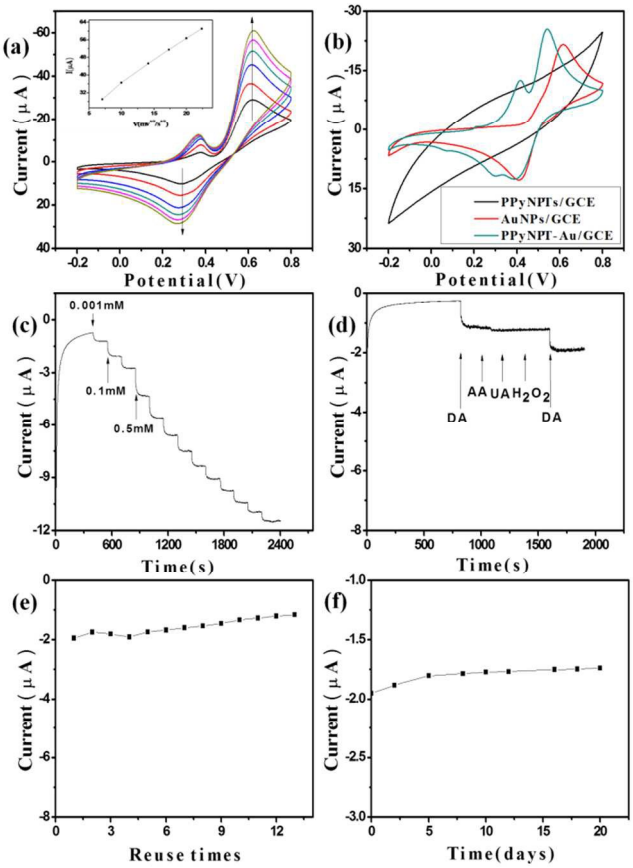

Fig. 8 DA sensor: (a) CVs of GCE modified with PPyNPT-Au in H_2SO_4 (pH 1) solution at different scanning rates. The inset is the calibration plot between current and scanning rate; (b) CVs of GCEs modified with AuNPs, PPyNPTs and PPyNPT-Au in the presence of 1 mM DA at a scan rate 50 mV s^{-1}; (c) I–T response; (d) Selectivity; (e) Reuse ability, and (f) Long-term stability.

Table.2. Comparison of the DA sensor performances of the PPyNPT-Au nanohybrids with previous DA sensors.

Electrode materials	Method	Linear range (mM)	LOD (μ M)	Ref
Nano-MnOOH	DPV	1.2×10^{-3}-0.2	0.1	56
Graphene-Pt	DPV	3×10^{-5}-8.13×10^{-3}	0.03	57
PPy-RGO	DPV	1×10^{-5}-0.01	1×10^{-6}	58
RGO-AuNPs	DPV	1×10^{-3}-0.06	2×10^{-5}	59
Au-graphene	AM	1×10^{-3}-0.321	0.32	60
PPyNPT-Au	AM	1×10^{-3}-5.201	0.36	this work

DPV: Differential pulse voltammetry
RGO: Reduced graphene oxide
AM: Amperometry

4 Conclusions

In summary, we demonstrated a facile synthesis of PPyNPTs by the polymerization of Py molecules, and further the as-prepared Ag and AuNPs were successfully assembled onto the created PPyNPTs for final synthesis of PPyNPT-Ag and PPyNPT-Au nanohybrids. In addition, we studied the effect of experimental parameters in the synthesis of PPyNPT-Ag and PPyNPT-Au nanohybrids and found the best reaction condition. At the end, both the nanohybrids were utilized to modify GCE for the fabrication of H_2O_2 and DA sensors. We found that the PPyNPT-Ag and PPyNPT-Au modified GCEs showed enhanced electrocatalytic activity for the reduction of H_2O_2 and oxidation of DA compared to PPyNPTs modified GCE, and the sensors based on PPyNPT-Ag and PPyNPT-Au can be used to detect H_2O_2 and DA, respectively.

Acknowledgment

The authors gratefully acknowledge the financial supports from the Fundamental Research Funds for the Central Universities (project no. ZZ1307).

Notes and references

[a]*State Key Laboratory of Chemical Resource Engineering, Beijing University of Chemical Technology, 100029 Beijing, China. E-mail: suzq@mail.buct.edu.cn*
[b]*Hybrid Materials Interface Group, Faculty of Production Engineering, University of Bremen, D-28359 Bremen, Germany. E-mail: wei@uni-bremen.de*

1. K. Dutta, S. Das, D. Rana and P. P. Kundu, *Polym. Rev.*, 2015, **55**, 1-56.
2. P. Santhosh, A. Gopalan and K. P. Lee, *J. Catal.*, 2006, **238**, 177-185.
3. J. Ding, K. Zhang, W. Xu and Z. Su, Nano, 2015, DOI: 10.1142/S1793292015501155.
4. K. E. Hnida, R. P. Socha and G. D. Sulka, *J. Phys. Chem. C*, 2013, **117**, 19382-19392.
5. A. G. MacDiarmid, *Angew. Chem., Int. Ed.*, 2001, **40**, 2581-2590.
6. J. Jang, *Adv. Polym. Sci.*, 2006, **199**, 189-260.
7. A. Babakhanian, S. Kaki, M. Ahmadi, H. Ehzari and A. Pashabadi, *Biosens. Bioelectron.*, 2014, **60**, 185-190.
8. P. Novák, K. Müller, K. S. V. Santhanam and O. Haas, *Cemh. Rev.*, 1997, **97**, 207-282.
9. X. Lu, Y. Li, J. Du, X. Zhou, Z. Xue, X. Liu and Z. Wang, *Electrochim. Acta*, 2011, **56**, 7261-7266.
10. Y. Z. Long, M. M. Li, C. Gu, M. Wan, J. L. Duvail, Z. Liu and Z. Fan, *Prog. Polym. Sci.*, 2011, **36**, 1415-1442.
11. P. Zhang, H. Wang, X. Zhang, W. Xu, Q. Li, G. Wei and Z. Su, *Biomater. Sci.*, 2015, **3**, 852-860.
12. Z. Ouyang, J. Li, J. Wang, Q. Li, T. Ni, X. Zhang, H. Wang, Q. Li, Z. Su and G. Wei, *J. Mater. Chem. B*, 2013, **1**, 2415-2424.
13. P. Zhang, Y. Huang, X. Lu, S. Zhang, J. Li, G. Wei and Z. Su, *Langmuir*, 2014, **30**, 8980-8989.
14. X. Zhao, P. Zhang, Y. Chen, Z. Su and G. Wei, *Nanoscale*, 2015, **7**, 5080-5093.
15. Y. Li, X. Zhao, P. Zhang, J. Ning, J. Li, Z. Su and G. Wei, *J. Mater. Chem. C*, 2015, **3**, 4126-4133.
16. Z. Su, J. Ding and G. Wei, *RSC Adv.*, 2014, **4**, 52598-52610.
17. L. Cui, J. Shen, F. Cheng, Z. Tao and J. Chen, *J. Power Sources*, 2011, **196**, 2195-2201.
18. J. Xu, J. Hu, B. Quan and Z. Wei, *Macromol. Rapid Commun.*, 2009, **30**, 936-940.
19. R. A. Vaia and J. F. Maguire, *Chem. Mater.*, 2007, **19**, 2736-2751.
20. J. R. Rau, S. C. Chen and H. W. Sun, *Electrochim. Acta*, 1994, **39**, 2773-2779.
21. J. Zhang, X. Liu, L. Zhang, B. Cao and S. Wu, *Macromol. Rapid Commun.*, 2013, **34**, 528-532.
22. X. Feng, H. Huang, Q. Ye, J. J. Zhu and W. Hou, *J. Phys. Chem. C*, 2007, **111**, 8463-8468.
23. E. Pintér, R. Patakfalvi, T. Fülei, Z. Gingl, I. Dékány and C. Visy, *J. Phys. Chem. B*, 2005, **109**, 17474-17478.
24. T. An, W. Choi, E. Lee, S. J. Cho and G. Lim, *J. Nanosci. Nanotechno.*, 2012, **12**, 4975-4978.
25. A. Chen, H. Wang and X. Li, *Chem. Commun.*, 2005, 1863-1864.
26. S. K. Pillalamarri, F. D. Blum and M. F. Bertino, *Chem. Commun.*, 2005, 4584-4585.
27. R. I. Chirita, C. West, A. L. Finaru and C. Elfakir, *J. Chromatogr. A*, 2010, **1217**, 3091-3104.

28. P. Diao, H. Yuan, F. Huo, L. Chen, D. Xiao, M. C. Paau and M. M. F. Choi, *Talanta*, 2011, **85**, 1279-1284.
29. J. Ding, S. Zhu, T. Zhu, W. Sun, Q. Li, G. Wei and Z. Su, *RSC Adv.*, 2015, **5**, 22935-22942.
30. P. Zhang, X. Zhao, X. Zhang, Y. Lai, X. Wang, J. Li, G. Wei and Z. Su, *ACS Appl. Mater. Interfaces*, 2014, **6**, 7563-7571.
31. Z. Su, J. Ding, G. Wei and Z. Su, *RSC Adv.*, 2014, **4**, 52598-52610.
32. P. Zhang, X. Zhang, S. Zhang, X. Liu, Q. Li, Z. Su and G. Wei, *J. Mater. Chem. B*, 2013, **1**, 6525-6531.
33. S. Yao, J. Xu, Y. Wang, X. Chen, Y. Xu and S. Hu, *Anal. Chim. Acta*, 2006, **557**, 78-84.
34. Y. Xiao, H. X. Ju and H. Y. Chen, *Anal. Chim. Acta*, 1999, **391**, 73-82.
35. G. Wei, Y. Zhang, S. Steckbeck, Z. Su and Z. Li, *J. Mater. Chem.*, 2012, **22**, 17190-17195.
36. M. Zhang, Y. Li, Z. Su and G. Wei, *Polym. Chem.* 2015, DOI: 10.1039/C5PY00777A.
37. P. Zhang, X. Zhao, Y. Ji, Z. Ouyang, X. Wen, J. Li, G. Wei and Z. Su, *J. Mater. Chem. B*, 2015, **3**, 2487-2496.
38. J. Ding, W. Sun, G. Wei and Z. Su, *RSC Adv.*, 2015, **5**, 35338-35345.
39. S. Jing, S. Xing, L. Yu and C. Zhao, *Mater. Lett.*, 2007, **61**, 4528-4530.
40. A. Doron, E. Katz and I. Willner, *Langmuir*, 1995, **11**, 1313-1317.
41. S. Jiang, Y. Ma, G. Jian, H. Tao, X. Wang, Y. Fan, Y. Lu, Z. Hu and Y. Chen, *Adv. Mater.*, 2009, **21**, 4953-4956.
42. A. Z. Sadek, C. Zhang, Z. Hu, J. G. Partridge, D. G. McCulloch, W. Wlodarski and K. Kalantar-zadeh, *J. Phys. Chem. C*, 2009, **114**, 238-242.
43. V. Radmilovic, H. A. Gasteiger and P. N. Ross, *J. Catal.*, 1995, **154**, 98-106.
44. X. Li, M. Wan, Y. Wei, J. Shen and Z. Chen, *J. Phys. Chem. B*, 2006, **110**, 14623-14626.
45. J. Wilson, S. Radhakrishnan, C. Sumathi and V. Dharuman, *Sens. Actuators, B: Chem.*, 2012, **171–172**, 216-222.
46. D. Sazou and C. Georgolios, *J. Electroanal. Chem.*, 1997, **429**, 81-93.
47. V. P. Menon, J. Lei and C. R. Martin, *Chem. Mater.*, 1996, **8**, 2382-2390.
48. W. Zhao, H. Wang, X. Qin, X. Wang, Z. Zhao, Z. Miao, L. Chen, M. Shan, Y. Fang and Q. Chen, *Talanta*, 2009, **80**, 1029-1033.
49. W. Lu, F. Liao, Y. Luo, G. Chang and X. Sun, *Electrochim. Acta*, 2011, **56**, 2295-2298.
50. X. Qin, W. Lu, Y. Luo, G. Chang and X. Sun, *Electrochem. Commun.*, 2011, **13**, 785-787.
51. M. R. Mahmoudian, Y. Alias, W. J. Basirun and M. Ebadi, *Electrochim. Acta*, 2012, **72**, 46-52.
52. J. Wang, X. Zhao, J. Li, X. Kuang, Y. Fan, G. Wei and Z. Su, *ACS Macro Lett.*, 2014, **3**, 529-533.
53. N. F. Zakharchuk, B. Meyer, H. Henning, F. Scholz, A. Jaworksi and Z. Stojek, *J. Electroanal. Chem.*, 1995, **398**, 23-35.
54. X. Q. Lin and L. Zhang, *Anal. Lett.*, 2001, **34**, 1585-1601.
55. X. Feng, C. Mao, G. Yang, W. Hou and J. J. Zhu, *Langmuir*, 2006, **22**, 4384-4389.
56. X. Cao, X. Cai and N. Wang, *Sens. Actuators, B: Chem.*, 2011, **160**, 771-776.
57. C. L. Sun, H. H. Lee, J. M. Yang and C. C. Wu, *Biosens. Bioelectron.*, 2011, **26**, 3450-3455.
58. T. Qian, S. Wu and J. Shen, *Chem. Commun.*, 2013, **49**, 4610-4612.
59. S. Liu, J. Yan, G. He, D. Zhong, J. Chen, L. Shi, X. Zhou and H. Jiang, *J. Electroanal. Chem.*, 2012, **672**, 40-44.
60. W. Zhu, T. Chen, X. Ma, H. Ma and S. Chen, *Colloids Surf., B*, 2013, **111**, 321-326.